Structural basis for the novel mechanism of drug extrusion by a MATE multidrug transporter

Yoshiki Tanaka[1,7], Christopher J. Hipolito[2], Andrés D. Maturana[3], Koichi Ito[4], Teruo Kuroda[5], Takashi Higuchi[2], Takayuki Katoh[2], Hideaki E. Kato[1], Motoyuki Hattori[1,6], Kaoru Kumazaki[1], Tomoya Tsukazaki[1,6], Ryuichiro Ishitani[1]*, Hiroaki Suga[2]* and Osamu Nureki[1]*

[1]Department of Biophysics and Biochemistry, Graduate School of Science, The University of Tokyo, 2-11-16 Yayoi, Bunkyo-ku, Tokyo 113-0032, Japan; [2]Department of Chemistry, Graduate School of Science, The University of Tokyo, 7-3-1 Bunkyo-ku, Tokyo 113-0033, Japan; [3]Department of Bioengineering Sciences, Graduate School of Bioagricultural Sciences, Nagoya University, Furo-cho, Chikusa-ku, Nagoya, 464-8601, Japan; [4]Department of Medical Genome Sciences, Graduate School of Frontier Sciences, The University of Tokyo, Chiba, 277-8562, Japan; [5]Department of Genome Applied Microbiology, Graduate School of Medicine, Dentistry and Pharmaceutical Sciences, Okayama University, Tsushima, Okayama, 700-8530, Japan; [6]JST, PRESTO, 4-1-8 Honcho, Kawaguchi, Saitama, 332-0012, Japan; [7]Present address: Department of Medical Chemistry and Cell Biology, Faculty of Medicine, Kyoto University, Konoe-cho, Yoshida, Sakyo-ku, Kyoto, 606-8501, Japan

*To whom reprint requests should be addressed: Phone: +81-3-5841-4392; E-mail: nureki@biochem.s.u-tokyo.ac.jp, Phone: +81-3-5841-8372; E-mail: hsuga@chem.s.u-tokyo.ac.jp, or +81-3-5841-4393; E-mail: ishitani@biochem.s.u-tokyo.ac.jp

MATE (multidrug and toxic compound extrusion) family transporters are conserved in the three primary kingdoms, and export xenobiotics using an electrochemical gradient of H^+ or Na^+ across the membrane[1,2]. MATE transporters confer multidrug resistance (MDR) to bacterial pathogens[3-6] and cancer cells[7], thus causing critical reductions in the therapeutic efficacies of antibiotics and anti-cancer drugs, respectively. Therefore, the development of MATE inhibitors has long been awaited in the field of clinical medicine[8,9]. Here we present the crystal structures of the H^+-driven MATE transporter from *Pyrococcus furiosus* in two distinct apo-form conformations, and in complexes with a derivative of the antibacterial drug norfloxacin and three *in vitro* selected thioether-macrocyclic peptides, at 2.1–3.0 Å resolutions. The structures, combined with functional analyses, revealed that the protonation of Asp41 on the N-terminal lobe induces the bending of TM1, which in turn collapses the N-lobe cavity, thereby extruding the substrate drug to the extracellular space. Moreover, the macrocyclic peptides bind the central cleft in distinct manners, which correlate with their inhibitory activities. The strongest inhibitory peptide that occupies the N-lobe cavity may pave the way toward the development of efficient inhibitors against MATE transporters.

Cellular export of toxic compounds is an essential process to maintain life[10-12]. MATE transporters function in the efflux of endogenous cationic, lipophilic substances and xenobiotics, and are ubiquitously distributed in archaea, bacteria, and eukarya. Bacterial MATE transporters confer multidrug resistance (MDR) to pathogens, such as multi-antibiotic resistant *Staphylococcus aureus*, which has attracted broad attention as a nosocomial infection. In cancer cells, MATE transporters export structurally diverse anti-cancer drugs, causing fatal reductions in the therapeutic efficacies of anti-cancer drugs. Thus, the demand for the discovery of molecules capable of antagonizing the functions of MATE transporters is quite high because of their clinical importance, but the screening campaigns for such drug leads have achieved very little success.

The MATE transporter, NorM, was identified from *Vibrio parahaemolyticus* as a Na^+/drug antiporter[13-15]. The crystal structures of NorM from *Vibrio cholerae* (NorM-VC) in the outward-open conformation was reported at 3.65 Å resolution[16]. This structure consists of 12 transmembrane-helices (TMs) forming two pseudo-symmetrical lobes, presenting a monovalent cation-binding site within the cavity in the C-terminal lobe, and a rocker-switch mechanism similar to that employed by the major facilitator superfamily (MFS) transporters[17] was proposed. However, due to the limited resolution, the structural mechanism of the cation influx and the drug efflux coupling, as well as

that allowing the recognition of a broad range of substrates, remained elusive.

A fluorescence-based analysis revealed that the MATE from *Pyrococcus furiosus* (PfMATE) is driven by a H^+ gradient, unlike NorM (Supplementary Discussion). PfMATE was crystallized using the lipidic cubic phase (LCP) method[18]. The crystals grown in LCP diffracted X-rays to 2.1 Å resolution at maximum. The co-crystallization with the cyclic peptide MaL6 (generated by the RaPID system[19-22], see below) improved the quality of the SeMet-derivatized crystals, which facilitated the phase determination by the single anomalous dispersion method. Finally, we determined the outward-open apo structures in two different conformations ("straight" and "bent" conformations at 2.4 and 2.5 Å resolutions, respectively) (Fig. 1a).

The structure of PfMATE consists of an N-lobe (TM1-TM6) and a C-lobe (TM7-TM12), which are related by a pseudo two-fold symmetry axis. The PfMATE structure adopts a V-shaped conformation, with the central cleft open toward the extracellular side, representing an outward-open state. Thus, the overall conformation of H^+-driven PfMATE is similar to that of Na^+-driven NorM-VC[23], which shares ~22% sequence identity with PfMATE (Supplementary Figs. 1 and 2, Supplementary Discussion). A large, hydrophobic central cleft, formed between the N- and C-lobes, can be divided into two cavities, the N- and C-lobe cavities. The N-lobe cavity is larger than

the C-lobe cavity (Fig. 1a). In NorM-VC, Glu255, Phe259, Tyr367, Asp371 and Phe429 recognize Rb^+ or Cs^+ in the C-lobe cavity (Supplementary Fig. 2b)[16]. These residues are not conserved in PfMATE, in which Met260, Phe279 and Trp283 occupy the cation-binding space (Supplementary Fig. 2c). Therefore, different cation-conducting pathways are likely utilized by the H^+-driven and Na^+-driven MATE transporters.

Although the present structures of PfMATE are essentially in the outward-open state, we found that it adopts two distinct conformations, the "bent" and "straight" conformations, in terms of the structure of the TM1 helix in the N-lobe (Fig. 1b, c and Supplementary Fig. 3a). The bent form crystals appeared around pH 6.0, while those of the straight form were obtained at pH 7.0-8.0. In the straight conformation, TM1 forms a single, straight helix, whereas in the bent conformation, it is kinked at Pro26 and Gly30, and bent toward the TM2 side (Fig. 1b and Supplementary Fig. 3b, c). Furthermore, in the bent conformation, the extracellular halves of the TM5 and TM6 helices and their connecting loop are slightly shifted outward by 9.9˚, and thus adopt a more outward-open conformation (Fig. 1a, Supplementary Movies). As a consequence, the N-lobe cavity, which is mainly formed between TM1 and TM2, is collapsed in the bent conformation (Fig. 1c, Supplementary Movies). To investigate the importance of Pro26, we mutated Pro26 to Ala and Ile, which remarkably reduced the EtBr and H^+

transport activities in the fluorescence-based analysis (Fig. 2a). On the other hand, the P26G and G30A mutants exhibited normal antiport activities (Fig. 2a). The results of the complementation assay also revealed that the P26A mutant could not complement the norfloxacin efflux activity (Fig. 2b). The membrane expression of all of the mutants was confirmed (Supplementary Fig. 4a). We also determined the crystal structure of P26A mutant at pH 6.5. The structure adopts the straight conformation even under the low-pH conditions, supporting the importance of Pro26 for the bending of TM1 (Supplementary Fig. 5). Thus, TM1 is kinked at Pro26 in the bent conformation, which is crucial for the drug export activity.

A drastic rearrangement of the side chain interactions was also observed between the straight and bent conformations, near the N-lobe cavity. Hydrophilic and acidic residues are clustered at the apex of the N-lobe cavity (Fig. 1b). In the straight conformation, the side chain of Asp184 (TM5) forms water-mediated hydrogen bonds with Tyr37, Asn180, and Thr202 (Fig. 1b and Supplementary Fig. 3c). Moreover, the Oδ atom of Asp184 is within hydrogen bonding distance (2.8 Å) with the Oδ atom of Asp41 (TM1), suggesting that the carboxylate group of either Asp41 or Asp184 is protonated. Given that Asp184 protrudes into the protein core, while Asp41 is exposed to the bulk solvent, it is likely that Asp184 is protonated and Asp41 is deprotonated. In contrast, in

the bent conformation, Asp41 (TM1) is closer to TM2, and its carboxylate group forms direct hydrogen bonds with Tyr139 (TM4) and Thr202 (TM6) (Fig. 1b and Supplementary Fig. 3c). Asp184 (TM5) again forms a direct hydrogen bond with Asp41. Thus, a tight water-mediated hydrogen-bond network between the side chains of Asp41, Asn180, Asp184, and Thr202 and the main-chain carbonyl of Ala198 (TM6) is formed (Fig. 1b and Supplementary Fig. 3c). This interaction network is further surrounded by the hydrophobic environment, and sequestered from the solvent region of the extracellular half channel (Supplementary Fig. 3d). Therefore, in the bent conformation, the Asp41 and Asp184 side chains are probably both protonated, since a charged group in such a low-dielectric environment inside the protein is energetically unfavorable. This is consistent with the fact that the bent form crystals appeared under acidic conditions. Moreover, a new hydrogen bond is formed between the side chains of Gln34 (TM1) and Asn154 (TM4) (Supplementary Fig. 3c). To investigate the importance of these acidic and hydrophilic residues in the N-lobe cavity, we performed fluorescence-based and complementation assays of the Asp41 and Asp184 mutants. These mutations abolished both the drug and H^+ transport activities (Fig. 2 and Supplementary Figs. 4c, d), indicating the importance of these acidic residues for the antiport mechanism. Furthermore, the Ala mutations of Tyr139 and Asn180 also

significantly reduced the transport activity (Fig. 2 and Supplementary Figs. 4c, d). Taken together, the present structures suggested that only the Asp184 side chain is protonated in the straight conformation, whereas Asp41 and Asp184 are both protonated in the bent conformation. The change in the protonation state of the Asp41 side chain may trigger the reorganization of the interaction network, thereby inducing the structural conversion between the straight and bent conformations (Supplementary Movies).

In the straight conformation, the lipid or monoolein molecules used in the crystallization bind to the N- and C-lobe cavities, and may mimic hydrophobic drug substrates, while the N-lobe cavity is collapsed in the bent conformation, and no density peaks were observed (Fig. 3a and Supplementary Fig. 6). To further investigate the drug recognition mechanism, we determined the 2.9 Å resolution crystal structure of PfMATE in the presence of a norfloxacin derivative compound (Br-NRF)[24], in which the 6-fluoro group of norfloxacin is replaced by bromine. The efflux of this compound by PfMATE was confirmed by the fluorescence-based assay (Supplementary Fig. 4c). In this structure, no lipid-like density was observed in the N-lobe cavity. Instead, an electron density that resembled the shape of the Br-NRF molecule was observed (Fig. 3b, c). The Br-NRF molecule is mainly recognized by shape complementarity, involving

the side chains of Gln34, Tyr37 (TM1), Asn153 (TM4), Met173, Ser177 (TM5), Thr202, Ser205, Met206, Thr209 and Ile213 (TM6). The 4-oxo group, the amine group of the 7-piperazine moiety and the 3-carboxylate group of Br-NRF are further recognized by hydrogen bond interactions with the side chains of Gln34 (TM1), Asn157 (TM4) and Asn180 (TM5), respectively (Fig. 3c). It should be noted that Tyr37, Asn180, and Thr202 are also involved in the hydrogen-bond network at the apex of the N-lobe cavity, as described above. To further explore the roles of these residues in the substrate recognition, we performed fluorescence-based and complementation assays of their mutants. The Ala mutants of Met173, Asn180 and Met206 abolished both the EtBr and H^+ transport activities (Fig. 2 and Supplementary Figs. 4c, d), indicating the importance of these residues for the recognition of the drug substrate. Intriguingly, the S177L and M206W mutants retained considerable H^+ transport activities, but showed significantly reduced EtBr transport activities (Fig. 2), thus exhibiting the decoupling of H^+ and EtBr transport.

To further investigate the drug efflux mechanism of PfMATE and to identify chemicals that antagonize the PfMATE activity, we performed an *in vitro* selection of thioether-macrocyclic peptides (MaL6, MaD5 and MaD3S; Fig. 4a and Supplementary Fig. 7a–c; Supplementary Discussion) that specifically interact with PfMATE, using the

RaPID (Random non-standard Peptide Integrated Discovery) system[19-22]. We analyzed the inhibitory activities of these cyclic peptides by fluorescence-based analyses using *E. coli* cells and outer membrane-stripped spheroplasts (Fig. 4b and Supplementary Fig. 8d). The PfMATE structures in complex with these cyclic peptides were also determined at 2.5, 3.0 and 2.6 Å resolutions, respectively (Fig. 4c and Supplementary Fig. 7d–f). The MaD5 peptide, which exhibited the highest inhibitory activity observed in the ethidium bromide-extrusion fluorescence-monitoring assay (Fig. 4b and Supplementary Fig. 8a), has a lariat-like structure consisting of a 7-aa minicycle head with a 13-aa linear tail (Fig. 4a and Supplementary Fig. 7a, d). In the complex crystal structure, PfMATE adopts the straight conformation, and the MaD5 peptide is deeply bound within the central cleft (Supplementary Fig. 7d). The peptide residues in the minicycle head fill the N-lobe cavity, which is involved in the recognition of the drug substrate. The C-terminal 8 residues of the 13-aa long tail were disordered and not visible in the crystal structure. On the other hand, the MaD3S peptide, which has the same small cyclic head structure but possesses a 9-aa tail with a different sequence composition from the MaD5 tail sequence (Fig. 4a and Supplementary Fig. 7b), exhibited lower inhibitory activity than that of the MaD5 peptide in the fluorescence-based assay (Fig. 4b and Supplementary Fig. 8b). Therefore, given that the

sequences and structures of the minicycle heads of MaD5 and MaD3S are the same, the 13-aa long tail of MaD5 has a significant impact on the inhibitory activity. The long MaD5 tail may restrict the rocker-switch motion of the N- and C-lobes, thereby contributing to the strong inhibitory activity of the MaD5 peptide. Then, to confirm the outer-membrane permeability of the MaD5 peptide, we stained MATE-positive *E. coli* cells using the fluorescent-labeled MaD5 peptide (Supplementary Fig. 9). The result suggested that these anti-MATE inhibitory peptides are able to penetrate the bacterial outer-membrane possibly via porin channels or other passive mechanisms, and reach the MATE protein embedded in the inner-membrane, thereby inhibiting the extrusion function (Fig. 4b and Supplementary Fig. 8). Thus, these peptides may provide new scaffolds for the development of potent inhibitors against MATE transporter families from bacteria and eukaryotes, thus impacting the treatments of MDR pathogens and MDR cancer cells.

The present analyses allowed us to propose the last step of the H^+-driven drug extrusion mechanism by MATE (Supplementary Fig. 10 and Supplementary Movies). Immediately after the structural conversion from the inward-open to outward-open state, the transporter is deprotonated, and only the drug substrate is bound to the transporter (state 1 in Supplementary Fig. 10, corresponding to the present Br-NRF complex

structure). After the protonation of Asp41, its side chain becomes sequestered within the hydrophobic environment, thereby inducing the bending of TM1 at Pro26, which collapses the N-lobe cavity and extrudes the bound drug substrate into the extracellular space (state 2 in Supplementary Fig. 10, corresponding to the present bent form structure). Finally, the protonated and substrate-unloaded transporter undergoes further structural conversion to the inward-open state (states 3-5 in Supplementary Fig. 10). During the review process, the crystal structures of Na^+- and substrate-bound NorM from *Neisseria gonorrheae* were reported at 3.5–3.6 Å resolutions[25], which may represent the intermediate state during the extrusion of the substrate based on our above mechanism. The complete understanding of the H^+/drug antiport cycle of MATE awaits the elucidation of the structures capturing the occluded and inward-open states.

Methods Summary

PfMATE was expressed in *E. coli* C41 cells. The cells were disrupted, and the membrane fraction was collected by ultracentrifugation. The protein was solubilized with DDM and purified by Ni^{2+}-affinity chromatography, followed by gel-filtration chromatography in the presence of Cymal-6. PfMATE was mixed with liquefied monoolein and crystallized in reservoir solutions (28–32% PEG400, 50 mM MES-NaOH, 20 mM $CaCl_2$, 100 mM NaSCN; pH 6.5). SeMet derivatives were prepared in *E. coli* C41 Met^- cells. The SeMet protein was mixed with the cyclic-peptide MaL6 and crystallized. X-ray diffraction datasets were collected by the helical data collection method[26] on beamline BL32XU at SPring-8. The crystal structure of PfMATE was determined by the single anomalous diffraction (SAD) method.

For the fluorescent analysis, spheroplasts of *E. coli* ΔacrB expressing PfMATE were incubated with 5 μM BCECF-AM (the acetoxymethyl ester permeates cells, while the hydrolyzed BCECF cannot permeate the cell membrane and accumulates within the cell)[27] and 100 μM norfoxacin for 30 min at room temperature. The spheroplasts were centrifuged briefly, and placed on glass coverslips under a confocal microscope (FV1000, Olympus, Japan). BCECF fluorescence was measured with excitation at 490 nm and emission at 530 nm. To reduce the external pH to 5.5, 10 mM MES was added.

The protonophore carbonyl cyanide m-chlorophenylhydrazone (CCCP) was then added at 50 μM, to equilibrate the intracellular and extracellular pH.

The selection of PfMATE-binding cyclic peptides and the chemical synthesis of the peptides were performed according to the RaPID system protocols[19-22]. The inhibitory activities of the macrocyclic peptides were investigated by EtBr accumulation, according to the literature[28]. EtBr (50 μM final concentration) was added to *E. coli* ΔacrB cells expressing PfMATE, in the presence of peptide, and the fluorescence emissions of the controls and the peptide-PfMATE mixtures were immediately measured by a Flexstation 3 (Molecular Devices).

Acknowledgements

We are grateful to the beam-line staff at BL32XU of SPring-8 for assistance in data collection, and the RIKEN BioResource Center (Ibaraki, Japan) for providing the *Pyrococcus furiosus* genomic DNA. This work was supported by the Japan Society for the Promotion of Science (JSPS) through its “Funding Program for World-Leading Innovative R&D on Science and Technology (FIRST program)” to O.N., by the Core Research for Evolutional Science and Technology (CREST) Program ‘The Creation of Basic Medical Technologies to Clarify and Control the Mechanisms Underlying

Chronic Inflammation' of Japan Science and Technology Agency (JST) to O.N., by a grant for HPCI STRATEGIC PROGRAM Computational Life Science and Application in Drug Discovery and Medical Development by MEXT to R.I., and by a Grant-in-Aid for Scientific Research (S) and a Grant-in-Aid for Young Scientists (A) from the Ministry of Education, Culture, Sports, Science and Technology (MEXT) to O.N. and R.I., respectively. This work was also supported by a JSPS Grant-in-Aid for the Specially Promoted Research (21000005) and MEXT Platform for Drug Discovery, Informatics, and Structural Life Science to H.S., and a Grant-in-Aid for JSPS post-doctoral fellows to C.J.H. (P11344).

Author contributions

Y.T. expressed and purified PfMATE for crystallization, collected the diffraction data, solved the structures and made the mutants for functional analyses. C.J.H. performed selections, syntheses and inhibition assays of macrocyclic peptides. A.D.M. performed the fluorescence analysis. K.I. performed growth complementation tests. T.K. performed drug susceptibility tests. T.H. synthesized Br-NRF. K.K. and H.E.K. assisted with data collection. M.H. and T.T. contributed to the early stage of the project. Y.T., C.J.H., H.E.K., R.I. and O.N. wrote the manuscript. H.S. and O.N. directed and

supervised all of the research.

Author information

The authors declare that they have no competing financial interests. The coordinates and structure factors for the *Pyrococcus furiosus* apo MATE ("straight" and "bent" conformations), P26A mutant, BrNRF-bound MATE and peptide-bound MATEs have been deposited in the Protein Data Bank, under the accession codes 3VVN, 3VVO, 3W4T, 3VVP, 3VVQ, 3VVR and 3VVS, respectively.

Figure Legends

Fig. 1. Overall structures of PfMATE

a. Cartoon representations of the two conformations of PfMATE, viewed from the membrane and extracellular sides, with helices TM1-TM12 marked. The molecules are shown as ribbons with each helix colored as a rainbow, from the N terminus (blue) to the C terminus (purple). **b**. Close-up views of the interaction networks in the two forms at the apex of the N-lobe cavity. Hydrogen bonds are indicated by black dashed lines. **c**. Surface models viewed from the central cleft, highlighting the N-lobe cavity. All molecular graphics were created with the program CueMol (http://www.cuemol.org/).

Fig. 2. Mutational analyses of PfMATE

a. The proton influx and substrate efflux activities of the PfMATE mutants. The percentages of the fluorescent intensity decrease of BCECF (black) and ethidium bromide (gray) were calculated, as described in the Supplementary Information. The bar graph represents the % fluorescence per a period of time, i.e. 5 min after the addition of MES. Error bars indicate the standard deviations from experiments repeated five times. **b**. Growth complementation tests of ΔacrB strains harboring PfMATE mutant vectors,

in the presence and absence of quinolone antibacterial agents.

Fig. 3. Complex structure of PfMATE and drug substrate

a. Surface model representations of the central clefts in the straight and bent conformations, colored by the electrostatic potential ranging from blue (+20 *kT*/*e*) to red (–20 *kT*/*e*). Lipids are shown by green stick models. **b**. The PfMATE structure in the complex with Br-NRF. The bound Br-NRF molecule is shown by a space-filling model. **c**, Drug recognition site, with a $2F_o–F_c$ map contoured at 1.0 σ as a mesh within 2.5 Å. Br-NRF and the surrounding residues are shown by stick models. Hydrogen bonds are indicated by black dashed lines.

Fig. 4. Complex structures with the macrocyclic peptides

a. Schematic representations of the thioether-macrocyclic peptides generated by the RaPID system[19-22]. ^{D}F denotes D-α-phenylalanine. **b.** Inhibition of the PfMATE activity by the macrocyclic peptides. *E. coli* C41(DE3)ΔacrB cells expressing PfMATE were treated with different concentrations of peptides as indicated in the x-axis of graphs. Error bars indicate the standard deviations from triplicate experiments. Control is

DMSO without peptide. **c**. Surface models of PfMATE complexes with the macrocyclic peptides, viewed from the membrane (upper panels) and extracellular side (lower panels). The bound peptides are depicted by space-filling models.

References

1 Brown, M. H., Paulsen, I. T. & Skurray, R. A. The multidrug efflux protein NorM is a prototype of a new family of transporters. *Mol. Microbiol.* **31**, 394-395 (1999).

2 He, G. X. *et al.* An H^+-coupled multidrug efflux pump, PmpM, a member of the MATE family of transporters, from *Pseudomonas aeruginosa*. *J. Bacteriol.* **186**, 262-265 (2004).

3 Kaatz, G. W., McAleese, F. & Seo, S. M. Multidrug resistance in Staphylococcus aureus due to overexpression of a novel multidrug and toxin extrusion (MATE) transport protein. *Antimicrob. Agents Chemother.* **49**, 1857-1864 (2005).

4 McAleese, F. *et al.* A novel MATE family efflux pump contributes to the reduced susceptibility of laboratory-derived Staphylococcus aureus mutants to tigecycline. *Antimicrob. Agents Chemother.* **49**, 1865-1871 (2005).

5 Tsuda, M. *et al.* Oppositely directed H+ gradient functions as a driving force of rat H^+/organic cation antiporter MATE1. *Am. J. Physiol.* **292**, F593-598 (2007).

6 Becker, M. L. *et al.* Genetic variation in the multidrug and toxin extrusion 1 transporter protein influences the glucose-lowering effect of metformin in patients with diabetes: a preliminary study. *Diabetes* **58**, 745-749 (2009).

7 Minematsu, T. & Giacomini, K. M. Interactions of tyrosine kinase inhibitors with

organic cation transporters and multidrug and toxic compound extrusion proteins. *Mol. Cancer Ther.* **10**, 531-539 (2011).

8 Ito, S. *et al.* Potent and specific inhibition of mMate1-mediated efflux of type I organic cations in the liver and kidney by pyrimethamine. *J. Pharmacol. Exp. Ther.* **333**, 341-350 (2010).

9 Kusuhara, H. *et al.* Effects of a MATE protein inhibitor, pyrimethamine, on the renal elimination of metformin at oral microdose and at therapeutic dose in healthy subjects. *Clin. Pharmacol. Ther.* **89**, 837-844 (2011).

10 Dawson, R. J. & Locher, K. P. Structure of a bacterial multidrug ABC transporter. *Nature* **443**, 180-185 (2006).

11 Murakami, S., Nakashima, R., Yamashita, E., Matsumoto, T. & Yamaguchi, A. Crystal structures of a multidrug transporter reveal a functionally rotating mechanism. *Nature* **443**, 173-179 (2006).

12 Wasaznik, A., Grinholc, M. & Bielawski, K. P. Active efflux as the multidrug resistance mechanism. *Postepy Hig. Med. Dosw.* **63**, 123-133 (2009).

13 Morita, Y. *et al.* NorM, a putative multidrug efflux protein, of Vibrio parahaemolyticus and its homolog in *Escherichia coli*. *Antimicrob. Agents Chemother.* **42**, 1778-1782 (1998).

14 Morita, Y., Kataoka, A., Shiota, S., Mizushima, T. & Tsuchiya, T. NorM of *Vibrio parahaemolyticus* is an Na^+-driven multidrug efflux pump. *J. Bacteriol.* **182**, 6694-6697 (2000).

15 Otsuka, M. *et al.* Identification of essential amino acid residues of the NorM Na^+/multidrug antiporter in *Vibrio parahaemolyticus*. *J. Bacteriol.* **187**, 1552-1558 (2005).

16 He, X. *et al.* Structure of a cation-bound multidrug and toxic compound extrusion transporter. *Nature* **467**, 991-994 (2010).

17 Law, C. J., Maloney, P. C. & Wang, D. N. Ins and outs of major facilitator superfamily antiporters. *Annu. Rev. Microbiol.* **62**, 289-305 (2008).

18 Cherezov, V. Lipidic cubic phase technologies for membrane protein structural studies. *Curr. Opin. Struct. Biol.* **21**, 559-566 (2011).

19 Hipolito, C. J. & Suga, H. Ribosomal production and in vitro selection of natural product-like peptidomimetics: the FIT and RaPID systems. *Curr. Opin. Chem. Biol.* **16**, 196-203 (2012).

20 Hayashi, Y., Morimoto, J. & Suga, H. In vitro selection of anti-Akt2 thioether-macrocyclic peptides leading to isoform-selective inhibitors. *ACS Chem. Biol.* **7**, 607-613 (2012).

21 Yamagishi, Y. *et al.* Natural product-like macrocyclic N-methyl-peptide inhibitors against a ubiquitin ligase uncovered from a ribosome-expressed de novo library. *Chem. Biol.* **18**, 1562-1570 (2011).

22 Morimoto, J., Hayashi, Y. & Suga, H. Discovery of Macrocyclic Peptides Armed with a Mechanism-Based Warhead: Isoform-Selective Inhibition of Human Deacetylase SIRT2. *Angew. Chem. Int. Ed.* **51**, 3423-3427 (2012).

23 Altschul, S. F. *et al.* Protein database searches using compositionally adjusted substitution matrices. *FEBS J.* **272**, 5101-5109 (2005).

24 Koga, H., Itoh, A., Murayama, S., Suzue, S. & Irikura, T. Structure-activity relationships of antibacterial 6,7- and 7,8-disubstituted 1-alkyl-1,4-dihydro-4-oxoquinoline-3-carboxylic acids. *J. Med. Chem.* **23**, 1358-1363 (1980).

25 Lu, M. *et al.* Structures of a Na^+-coupled, substrate-bound MATE multidrug transporter. *Proc. Natl. Acad. Sci. U. S. A.* **110**, 2099-2104 (2013).

26 Flot, D. *et al.* The ID23-2 structural biology microfocus beamline at the ESRF. *J. Synchrotron Radiat.* **17**, 107-118 (2010).

27 Tsujimoto, K., Semadeni, M., Huflejt, M. & Packer, L. Intracellular pH of Halobacteria Can Be Determined by the Fluorescent Dye 2',

7'-Bis(Carboxyethyl)-5(6)-Carboxyfluorescein. *Biochem Bioph Res Co* **155**, 123-129 (1988).

28 Li, X. Z., Poole, K. & Nikaido, H. Contributions of MexAB-OprM and an EmrE homolog to intrinsic resistance of *Pseudomonas aeruginosa* to aminoglycosides and dyes. *Antimicrob. Agents Chemother.* **47**, 27-33 (2003).

Full Methods

Cloning, Expression and Purification

The PfMATE gene was cloned from *Pyrococcus furiosus* (strain ATCC 43587) and spliced into the expression vector pET11a (Novagen), between the *Nde*I and *Xho*I restriction sites of the multiple cloning site. The hexa-histidine tag (His_6-tag) was introduced at the C-terminus of the PfMATE construct. The pET11a-PfMATE plasmid was transformed into the *E. coli* C41(DE3)ΔacrB strain, constructed in-house. The cells were grown in a 5-liter culture at 37 °C to an absorbance at 600 nm (OD_{600}) of 0.5, and the gene expression was induced with 0.5 mM isopropyl β-D-thiogalactopyranoside (IPTG) at 20 °C for 12 h. The cells were pelleted by centrifugation at 4,000 g, and were disrupted by a Microfluidizer (Microfluidics). After centrifugation (25,000 g), the supernatant was ultra-centrifuged (200,000 g), and the membrane fraction was collected. The PfMATE was solubilized from the membrane fraction with n-dodecyl-β-D-maltopyranoside (DDM), and was purified by the following chromatography steps. The insoluble material was removed by

ultracentrifugation (Beckman Type 70 Ti rotor, 150,000 g, 30 min), and the supernatant was mixed with Ni-NTA resin (QIAGEN). The His_6-tag of the PfMATE was cleaved by 1 μg ml^{-1} trypsin (Invitrogen) at 4 °C overnight, and the protein was re-chromatographed on a Ni-NTA column. The His_6-tag-cleaved PfMATE was further purified by gel filtration (Superdex 200 10/300 GL, GE Healthcare) in 20 mM HEPES-NaOH, pH 7.0, containing 20 mM NaCl and 0.06% Cymal-6.

Crystallization

The purified protein was concentrated to about 8 mg ml^{-1} with a centrifugal filter device (Millipore 50 kDa MW cutoff), for crystallization. PfMATE was mixed with liquefied monoolein (Sigma) in a 2:3 protein to lipid ratio (w/w), using the twin-syringe mixing method. Aliquots (100 nl) of the protein-LCP mixture were spotted on a 96-well sandwich plate and overlaid with 1 μl of precipitant solution by the crystallization robot, mosquito LCP (TTP LabTech). Native crystals for data collection were grown at 20 °C in reservoir solutions (28-30% PEG400, 50 mM MES-NaOH, 20 mM $CaCl_2$, 100 mM NaSCN; pH 6.0-8.0). The crystals grew to full size within 5 to 7

days. The crystals were flash-cooled, using reservoir solution containing 32% PEG400 as a cryoprotectant, and were stored in liquid nitrogen. The substrate complex of Br-NRF was dissolved to a 100 mM concentration in 10 mM sodium acetate, pH 4.5, and was mixed with the protein solution at a 20:1 protein to drug ratio (v/v). For the thioether-macrocyclic peptide complexes, the macrocyclic peptides were dissolved in DMSO to a 20 mM concentration, and were mixed with the protein solution in a 20:1 protein to peptide ratio (w/w). Crystallization was performed as described above in reservoir solutions (26-28% PEG550MME, 100 mM Tris-HCl, 100 mM Li_2SO_4; pH 8.0). The P26A mutant was purified by gel filtration in 20 mM MES-NaOH, pH 6.0, containing 20 mM NaCl and 0.06% Cymal-6, and crystallization was performed as described above in reservoir solutions (30% PEG400, 50 mM MES, 100 mM NaSCN, 20 mM $CaCl_2$; pH 6.5).

Selenomethionine-derivatized PfMATE (SeMet PfMATE) was overexpressed in *E. coli* C41(DE3)Met^-, and was purified in the same manner as the native protein. The SeMet protein was mixed with the macrocyclic peptide MaL6, and incubated for 1 h at 4 °C. Crystals for data collection were grown at 20 °C by the LCP glass sandwich batch

method, using 1.0 μl reservoir solution (30–32% PEG400, 100 mM MES, 100 mM magnesium acetate; pH 6.5). The co-crystallization with MaL6 improved the quality and reproducibility of the crystals, especially in the crystallization of SeMet PfMATE, and thus facilitated the phase determination by the SAD method.

Data collection and structure determination

The crystal structure of PfMATE was determined by single anomalous dispersion (SAD) phasing, using the SeMet-derivatized PfMATE-MaL6 complex crystal. X-ray diffraction data sets were collected by the helical data collection method[26] on beamline BL32XU at SPring-8, using a micro beam with a 1-μm width and a 5-μm height[29]. The diffraction data were processed using the HKL2000 program suite (HKL Research). The heavy atom sites were identified with the program SnB[30]. The experimental phases were calculated using the program AutoSHARP[31]. The homology model, generated from NorM-VC (PDB accession code: 3MKU) with the program MODELLER[32], was fit to the initial experimental electron density map, and manually modified using the program Coot[33,34]. The model was refined with the programs

Phenix[35] and autoBUSTER[36]. The final models were examined by Ramachandran plots, using the program MolProbity[37]. The crystal structures of the native MATE and the complexes with the Br-NRF, MaL6, MaD5 and MaD3S peptides were determined by molecular replacement, using the program PHASER[38,39]. The best data set of the native MATE was refined with R_{work}/R_{free} = 21.7%/24.4% at 2.4 Å resolution (Supplementary Tables 1 and 2). The asymmetric units of the crystals of the native MATE and the peptide complex contain a single MATE molecule. The asymmetric unit of the drug complex contains two molecules. Molecular graphics were created with the program CueMol (http://www.cuemol.org/).

In vivo complementation assays

The drug-sensitive strain (BW25113) ΔacrB was transformed with each pSUIQ plasmid[40], and the transformants were obtained primarily on LB (7 μg ml^{-1} chloramphenicol) plates. Each colony was streaked on 0.02 μg ml^{-1} norfloxacin plates, and colony growth was monitored.

Generation of spheroplasts

Giant spheroplasts, which were large enough for fluorescence measurement by confocal microscopy, were generated by genetic and pharmacological procedures[41,42]. To generate the giant spheroplasts, cells were inoculated in 5 ml of LB medium (50 μg ml^{-1} ampicillin) in a 14 ml test tube, and were incubated at 37 ˚C aerobically by rotation at 200 r.p.m., until the OD_{600} reached 0.3–0.5. At the desired OD_{600}, a 5 ml portion of the exponentially growing culture was diluted 10-fold into 5 ml of pre-warmed LB medium, supplemented with 60 μg ml^{-1} cephalexin (SIGMA) to block cell division. After 3 h of incubation at 37 ˚C with rotation at 200 r.p.m., the un-septated filaments were harvested by centrifuging the entire culture at 3,000 g for 3 min. The filament pellet was then resuspended in 500 μl of 0.8 M sucrose, by pipetting. A 30 μl aliquot of 1 M Tris–HCl (pH 8.0), 24 μl of 0.25 mg ml^{-1} lysozyme (300 units, SIGMA #L6876), 6 μl of 5 mg ml^{-1} DNase I (SIGMA #D5025), and 6 μl 125 mM EDTA-NaOH (pH 8.0) were sequentially added and mixed immediately in between additions, by inverting the tube a few times. After an 8 min incubation at room temperature, a 100 ml aliquot of stop solution (10 mM Tris-HCl, pH 8.0, 0.7 M sucrose, 20 mM $MgCl_2$) was added to

terminate the cell wall digestion. The spheroplasts were frozen at –20 ˚C.

BCECF Fluorescence analysis

The changes in pH were monitored in spheroplasts, using the pH probe BCECF (2',7'-bis(2-carboxyethyl)-5(6)-carboxyfluorescein, Molecular Probes, Invitrogen, US). In summary, the spheroplasts were incubated with 5 μM BCECF-AM[27] and 100 μM norfoxacin for 30 min at room temperature. The spheroplasts were then centrifuged briefly (4,000 rpm, 5 min), and were placed on glass coverslips under a confocal microscope (FV1000, Olympus, Japan). The spheroplast medium was composed of 150 mM KCl, 20 mM $CaCl_2$, 5 mM HEPES and 300 mM sucrose (pH 7.5, KOH). BCECF fluorescence was observed with excitation at 488 nm and emission at 530 nm. The fluorescence intensity at time 0 was set as the maximum (100%), to avoid the spheroplast-to-spheroplast variability in fluorescent intensity. Spheroplasts on glass coverslips were randomly selected for fluorescence measurement. To reduce the external pH to 5.5, 10 mM MES was added. After the addition of MES, 50 μM of the protonophore CCCP (carbonyl cyanide-m-chlorophenylhydrazone) was added, to

equilibrate the intracellular and extracellular pH. Each graph has the mean and sem of n=8-15 spheroplasts (measured in 3-6 experiments with 1-5 spheroplasts measured for each experiment).

Ethidium bromide fluorescence analysis

To monitor drug export by MATE, spheroplasts were loaded with ethidium bromide (20 μM) for 40 min, and then washed by brief centrifugation (4,000 rpm for 5 min). The spheroplasts were suspended in 150 mM KCl, 20 mM $CaCl_2$, 5 mM HEPES and 300 mM sucrose (pH 7.5, KOH). Ethidium bromide fluorescence was observed with excitation at 490 nm and emission at 600 nm, using a confocal microscope (FV1000, Olympus, Japan). To generate a proton gradient, 10 mM MES was added, thus reducing the pH to 5.5. Each graph has the mean and sem of n=9-19 spheroplasts (measured in 3-6 experiments with 1-8 spheroplasts measured during each experiments).

Selection for binding cyclic peptides and chemical synthesis

The selection of PfMATE-binding cyclic peptides and the chemical synthesis of the selected peptides were performed according to the RaPID system protocols. Libraries were constructed using a random region consisting of 7-15 NNK codons. Translation initiation of the "L" library utilized chloroacetyl-L-phenylalanine-$tRNA^{init}_{CAU}$. Translation initiation of the "D" library utilized chloroacetyl-D-phenylalanine-$tRNA^{init}_{CAU}$. The selections performed at 4 °C and 37 °C were halted at the seventh and sixth rounds, respectively. The details of the construction and characterization of the PfMATE-binding cyclic peptides will be published in a separate report.

Inhibition Assay

The inhibitory activities of the MaL6, MaD5 and MaD3S peptides were tested by an ethidium bioaccumulation assay, according to the literature with modifications[28]. *E. coli* ΔacrB was used to express PfMATE. Cells containing the PfMATE expression

vector were grown in LB medium, containing 100 μg ml^{-1} ampicillin, overnight at 37 °C, with shaking at 200 rpm. A stationary phase *E. coli* culture was diluted 100-fold in fresh LB medium containing 100 μg ml^{-1} ampicillin. Cells were grown at 37 °C to an OD_{600} of 0.5, and expression was induced by the addition of IPTG (final concentration of 0.5 mM). The induced cells were incubated for 3 hours at 37 °C, with shaking at 200 rpm. The cells collected from 500 μl of induced culture were washed once with 50 mM Tris buffer (500 μl, pH 7.0), and resuspended in 50 mM Tris buffer (pH 7.0) to a final OD_{600} of 0.5. To the wells of a 96-well black plate (1/2 area, Perkin Elmer), a 44.5 μl portion of the above cell suspension was added to 0.5 μl of peptide, ranging in concentration from 0–2.5 mM in DMSO. For a positive control, 0.5 μl of a 10 mM solution of CCCP dissolved in DMSO was used, instead of the peptide dissolved in DMSO. EtBr (0.5 mM, 5 μl) was added to the *E. coli* cells mixed with the peptide, a blank negative control, or a CCCP positive control, and the plate containing the mixtures was immediately placed within the plate reader (Flexstation 3, Molecular Devices). Note that there was about a 15 second delay between the addition of EtBr and the first reading (t = 0 seconds). Fluorescence readings were taken at 30-second

intervals, from 0 to 900 seconds. Each trial contained 2.2 x 10^8 *E. coli* cells in a 50 µL final volume.

Method References

29 Hirata, K. *et al.* New micro-beam beamline at SPring-8, targeting at protein micro-crystallography. *AIP Conf. Proc.* **1234**, 901-904 (2010).

30 Xu, H., Smith, A. B., Sahinidis, N. V. & Weeks, C. M. SnB version 2.3: triplet sieve phasing for centrosymmetric structures. *J. Appl. Crystallogr.* **41**, 644-646 (2008).

31 Vonrhein, C., Blanc, E., Roversi, P. & Bricogne, G. Automated structure solution with autoSHARP. *Methods Mol. Biol.* **364**, 215-230 (2007).

32 Eswar, N. *et al.* Comparative protein structure modeling using MODELLER. *Curr. Protoc. Protein Sci.* **2**, 2.9.1-2.9.31 (2007).

33 Emsley, P. & Cowtan, K. Coot: model-building tools for molecular graphics. *Acta Crystallogr.* **D60**, 2126-2132 (2004).

34 Emsley, P., Lohkamp, B., Scott, W. G. & Cowtan, K. Features and development of Coot. *Acta Crystallogr D Biol Crystallogr* **66**, 486-501 (2010).

35 Adams, P. D. *et al.* PHENIX: a comprehensive Python-based system for macromolecular structure solution. *Acta Crystallogr.* **D66**, 213-221 (2010).

36 Smart, O. S. *et al.* Exploiting structure similarity in refinement: automated NCS and target-structure restraints in BUSTER. *Acta Crystallogr.* **D68**, 368-380 (2012).

37 Chen, V. B. *et al.* MolProbity: all-atom structure validation for macromolecular crystallography. *Acta Crystallogr.* **D66**, 12-21 (2010).

38 McCoy, A. J. *et al.* Phaser crystallographic software. *J. Appl. Cryst.* **40**, 658-674 (2007).

39 Zwart, P. H. *et al.* Automated structure solution with the PHENIX suite. *Methods Mol. Biol.* **426**, 419-435 (2008).

40 Ito, K., Ebihara, K., Uno, M. & Nakamura, Y. Conserved motifs in prokaryotic and eukaryotic polypeptide release factors: tRNA-protein mimicry hypothesis. *Proc. Natl. Acad. Sci. U. S. A.* **93**, 5443-5448 (1996).

41 Martinac, B., Buechner, M., Delcour, A. H., Adler, J. & Kung, C. Pressure-sensitive ion channel in Escherichia coli. *Proc. Natl. Acad. Sci. U. S. A.* **84**, 2297-2301 (1987).

42 Kuo, M. M., Saimi, Y., Kung, C. & Choe, S. Patch clamp and phenotypic analyses of a prokaryotic cyclic nucleotide-gated K^+ channel using *Escherichia coli* as a host. *J. Biol. Chem.* **282**, 24294-24301 (2007).

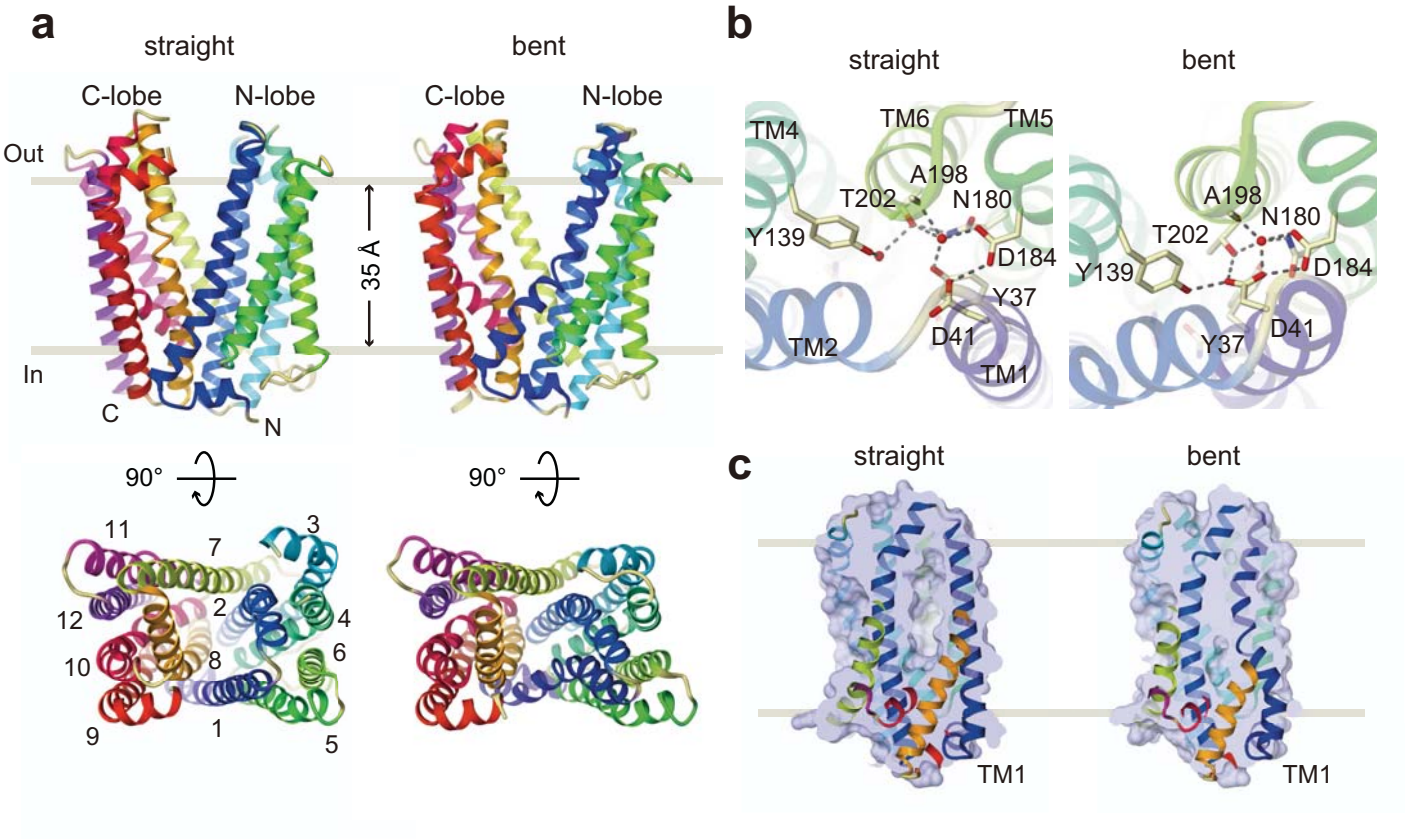

Tanaka et al. Figure 1

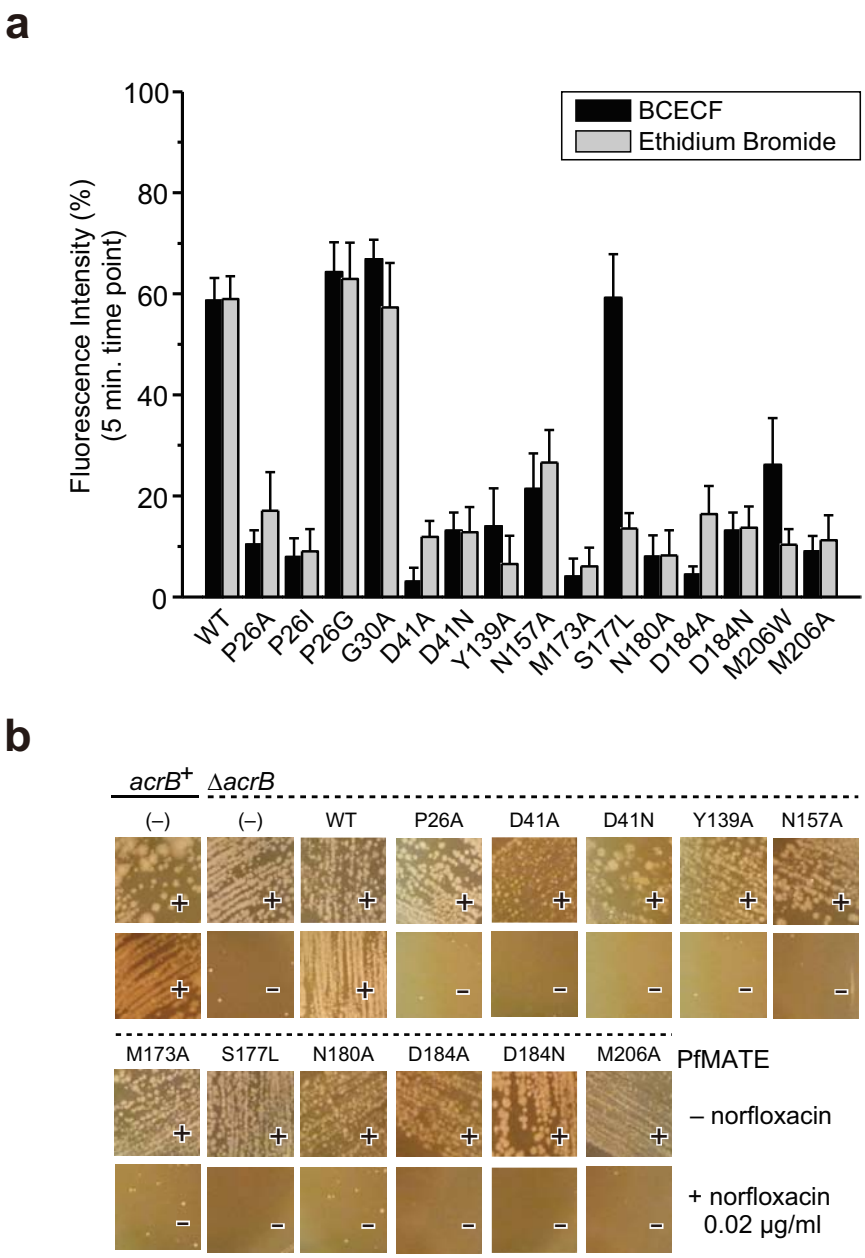

Tanaka et al. Figure 2

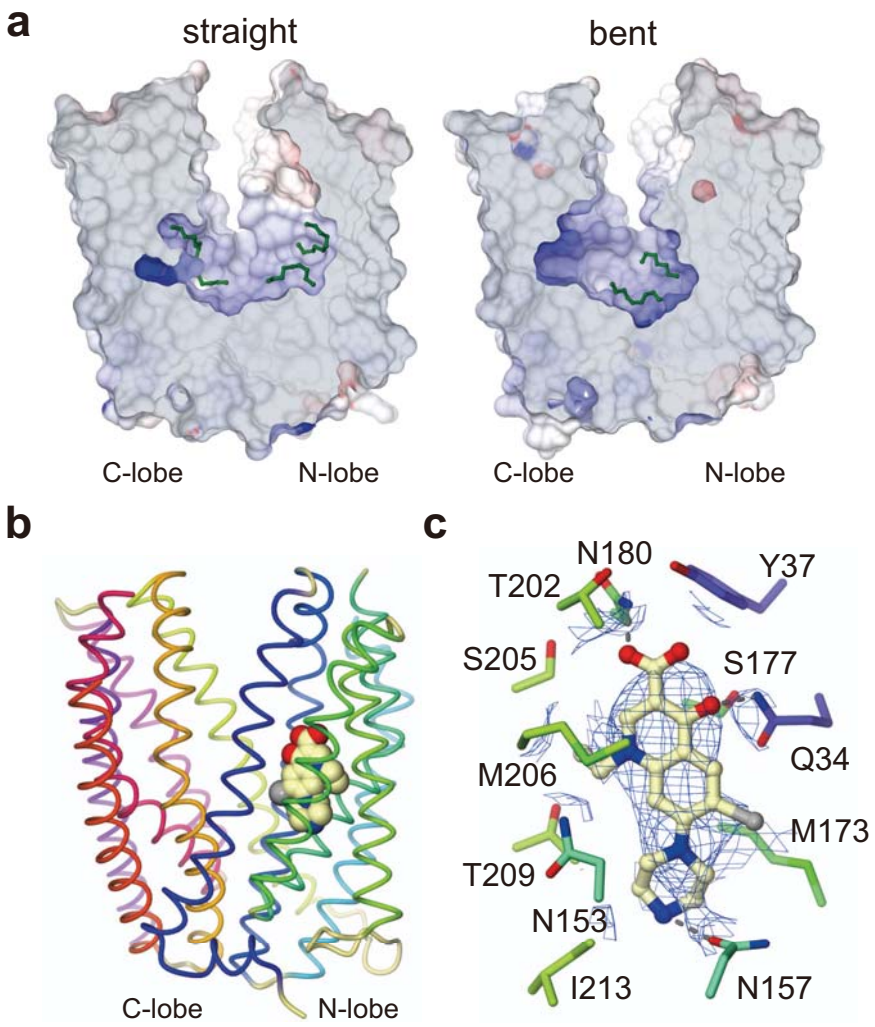

Tanaka et al. Figure 3

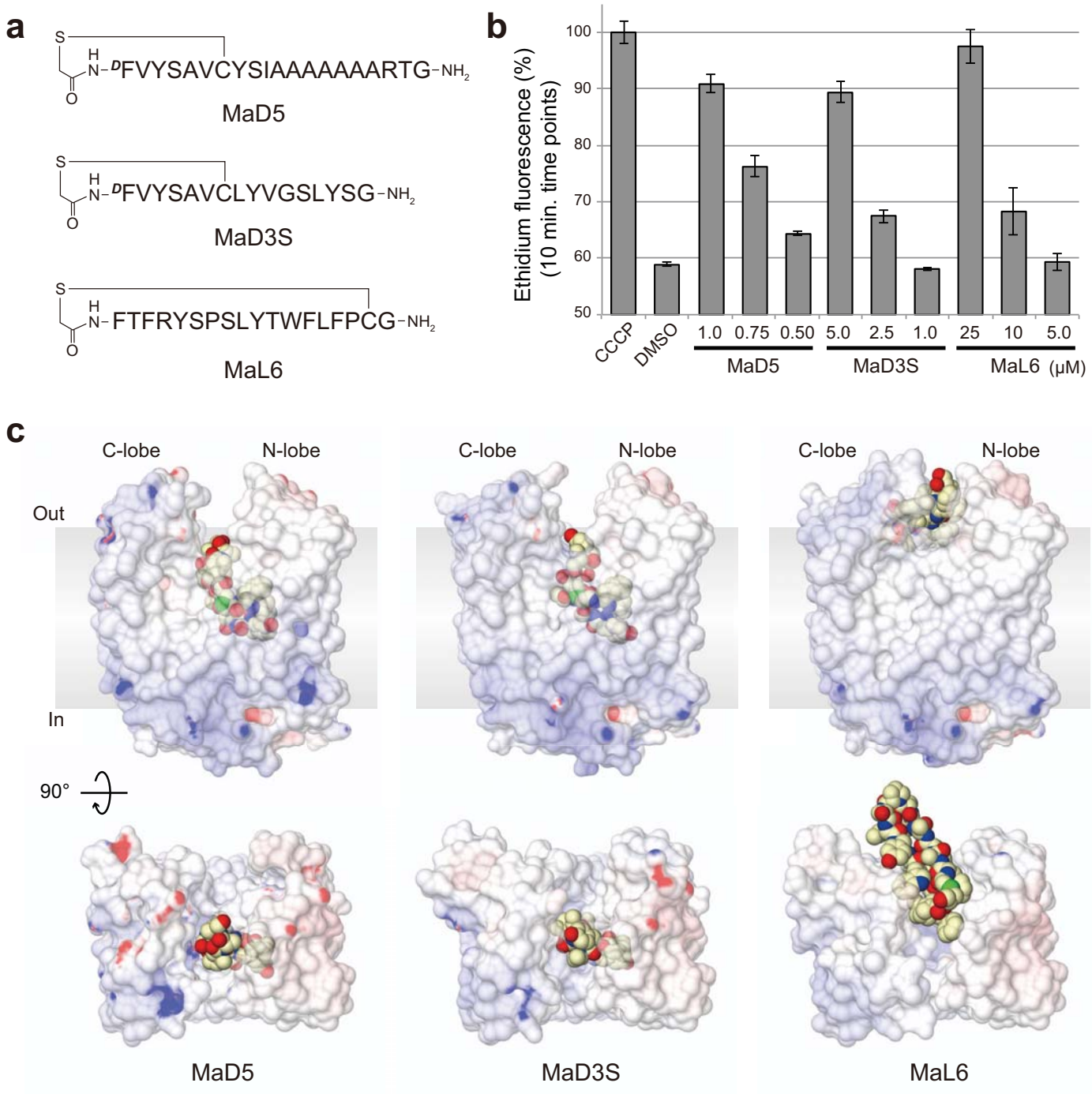

Tanaka et al. Figure 4